International Journal of Heat and Mass Transfer 51 (2008) 5590–5597

Contents lists available at ScienceDirect

International Journal of Heat and Mass Transfer

journal homepage: www.elsevier.com/locate/ijhmt

Microfluidics of nano-drug delivery

Clement Kleinstreuer [a,b,*], Jie Li [a], Junemo Koo [c]

[a] Department of Mechanical and Aerospace Engineering, North Carolina State University, Raleigh, NC 27695-7910, USA
[b] Department of Biomedical Engineering, North Carolina State University, Raleigh, NC 27695-7910, USA
[c] Department of Mechanical Engineering, Kyung Hee University, Seocheon-dong, Gyeonggi-do 446-701, South Korea

ARTICLE INFO

Article history:
Received 12 December 2007
Received in revised form 4 April 2008
Available online 12 June 2008

Keywords:
Bio-MEMS
Drug delivery
Nanofluids
Microfluidics
Microchannel

ABSTRACT

After a brief review of microfluidics, a bio-MEMS application in terms of nanofluid flow in microchannels is presented. Specifically, the transient 3-D problem of controlled nano-drug delivery in a heated microchannel has been numerically solved to gain new physical insight and to determine suitable geometric and operational system parameters. Computer model accuracy was verified via numerical tests and comparisons with benchmark experimental data sets. The overall design goals of near-uniform nano-drug concentration at the microchannel exit plane and desired mixture fluid temperature were achieved with computer experiments considering different microchannel lengths, nanoparticle diameters, channel flow rates, wall heat flux areas, and nanofluid supply rates.

Such micro-systems, featuring controlled transport processes for optimal nano-drug delivery, are important in laboratory-testing of predecessors of implantable smart devices as well as for analyzing pharmaceuticals and performing biomedical precision tasks.

1. Introduction

Microfluidics is the study of transport processes in microchannels, i.e., methods and devices for controlling and manipulating fluid flow and particle transport at the microscale. Microfluidic devices, consisting in general of reservoirs, channels, pumps, valves, mixers, actuators, filters and/or heat exchangers, are primary components of lab-on-a-chip and total analysis systems [1] or function as bio-MEMS for precise drug delivery by implanted or transdermal techniques. Larger versions may be used as micro-heat sinks in miniature electronic systems (see Kleinstreuer and Li, [2]). The basics of microfluidics are discussed in the books by Tabeling [3] and Nguyen and Wereley [4], while bio-MEMS fundamentals, technologies, and applications for drug delivery have been reviewed by Tay [5] as well as in selected chapters by Saliterman [6] and Wang and Soper [7]. Beebe et al. [8] summarized the physics and applications of microfluidics in biology, discussing microdevice components as well as manufacturing methods, such as micromachining, soft lithography, embossing, *in situ* construction, injection molding, and laser ablation. As Beebe et al. [8] illustrated, the main component in any microfluidic device is the channel network.

Bio-MEMS can be considered as having at least one system dimension in the submicron or micron range (100 nm–200 μm) and other dimensions of up to several millimeters [6]. With the increasing awareness of microfluidic physics and the surface science of building materials, such as silicon, polymers, glass and ceramics, the traditional fabrication techniques previously imported from integrated circuit manufacturing to MEMS have been also applied to bio-MEMS. The central question in microfluidics modeling is the validity of the continuum assumption, and if so (as may be the case for standard water flow in microchannels with $D_h > 0.1$ μm), which are the dominant forces? Important characteristics and phenomena in the microscale environment include laminar flow, entrance effects, surface roughness effects, diffusion, wall forces, surface tension, very high surface-area-to-volume ratio, and microfluidic resistance. For example, some experimental evidence indicates that the Reynolds number for transition from laminar to turbulent flow may be different in microchannels from that predicted by macrochannel-flow theory. Indeed, recent works analyzed by Koo and Kleinstreuer [9] showed that a lot of controversy exists between experimental reports on (thermal) microscale flows, explaining that surface roughness and entrance effects may cause early turbulence.

In the 1990s most bio-MEMS studies were concentrated in academia, while in recent years commercialization of such devices began. Examples include an electronically activated drug delivery microchip (Shawgo et al., [10]); a controlled delivery system via integration of silicon and electroactive polymer technologies; a MEMS-based DNA sequencer developed by Cepheid [11]; and

* Corresponding author. Address: Department of Mechanical and Aerospace Engineering, North Carolina State University, Raleigh, NC 27695-7910, USA. Tel.: +1 9195155261; fax: +1 9195157968.
E-mail address: ck@eos.ncsu.edu (C. Kleinstreuer).

0017-9310/$ - see front matter © 2008 Elsevier Ltd. All rights reserved.
doi:10.1016/j.ijheatmasstransfer.2008.04.043

Nomenclature

A_g	geometric area
A_v	valid area
c	concentration
c_p	specific heat capacity
d	diameter
D	diffusivity coefficient
D_h	hydraulic diameter
H	channel height
k	thermal conductivity
L	channel length
Nu	Nusselt number
p	pressure
Po	Poiseuille number
Pr	Prandtl number
q''	uniform heat flux
R_b	interface thermal resistance
Re	Reynolds number
T	temperature
t	time
u, v	velocity components
W	channel width

Greek symbols

α	aspect ratio
φ	volume fraction
κ_B	Boltzmann constant
μ	dynamic viscosity
ν	kinematic viscosity
ρ	density
χ	Reynolds number ratio

Subscripts

eff	effective
f	base fluid
p	particle

arrays of in-plane and out-of-plane hollow micro-needles for dermal/transdermal drug delivery (Ovsianikov et al., [12] and Kim and Lee, [13] among others) as well as nanomedicine applications of nanogels or gold-coated nanoparticles (Labhasetwar and Leslie-Pelecky, [14]). Part of the advanced endeavors in developing integrated micro- or nano-drug delivery systems is the interest in easily monitoring and controlling target-cell responses to pharmaceutical stimuli, to understand biological cell activities, or to facilitate drug development processes.

While micro-devices allow precise drug delivery by both implanted and transdermal techniques, conventional drug delivery is characterized by the "hill-and-valley" phenomenon. It implies that when a drug is dispensed, drug concentration in the blood will increase, peak and then drop as the drug is metabolized, where the cycle is repeated for each drug dose. In nano-drug delivery (ND) systems, controlled drug release occurs over an extended period of time. Hence, the desired drug concentration will remain within the therapeutic window as needed. Usually, an integrated ND system is composed of drug preparation, feeding, sensing (test), and feedback parts. The types and doses of drugs are selected in the drug preparation part, while the feeding system guides drugs and buffer fluids into the test part. Test cells are placed into the test section, where they react to drugs and resulting (electric) response signals are monitored via the feedback part.

Of interest here is the optimal delivery of nanoparticles (drugs) in an aqueous solution in terms of predetermined uniform particle concentration and mixture temperature. Such a dilute suspension, called a nanofluid, is conveyed via microchannels to recipient living cells situated in a well (see Fig. 1a). Controlled dosages of nano-drugs allow for simultaneous testing of living cells and stimuli responses. Those micro-systems, featuring controlled transport processes for optimal nano-drug delivery, are important in laboratory-testing of predecessors of implantable smart devices which may offer closed-loop sensing, result interpretation, and automatic nano-drug dispensation. Other applications for this basic microfluidic device include testing of pharmaceuticals and performing efficient biomedical analyses.

2. Theory

In the controlled multiple nano-drug-stream system (Fig. 1a), the plenum chamber functions as a reservoir of an aqueous nutrient-supply and/or purging fluid. The microchannels can alter the incoming fluid to the test section, i.e., target-well with living cells, by adjusting the individual inlet pressure or resistance. Nano-drugs can be supplied by setting the supply pressure of the nano-drug solution higher than that of the fluid supply side, while purging fluid can go through the testing section by lowering or eliminating the drug supply pressure. An appropriate wall heat flux beneath the microchannels ensures that delivery of the drug-fluid mixture to the living cells occurs at an optimal temperature, i.e., 37 °C. Due

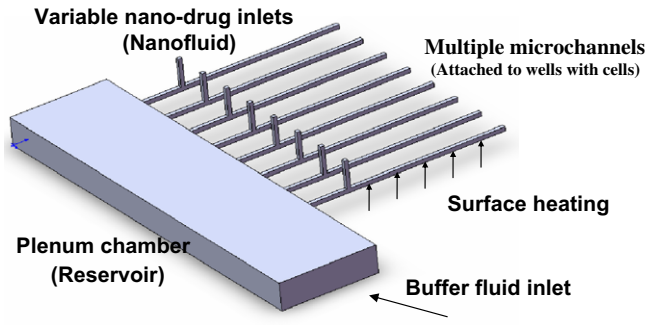

Fig. 1a. Nanomedicine delivery system with eight microchannels.

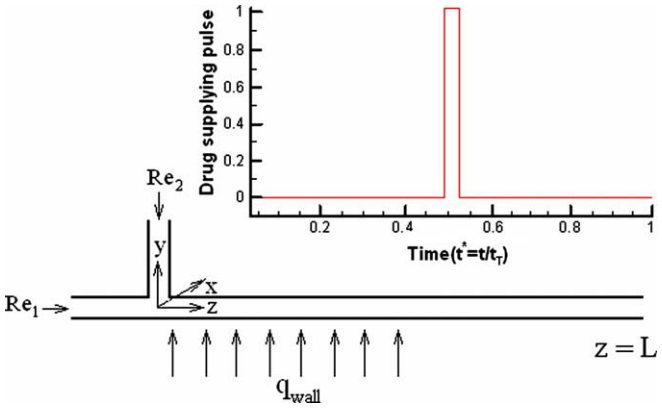

Fig. 1b. Representative microchannel with controlled nanofluid injection.

to the temperature dependent fluid properties, i.e., viscosity, density, diffusivity and thermal conductivity, the heat flux was also assumed to have an influence on the drug concentration and velocity distribution. Selecting one representative microchannel, the chosen unit has a hydraulic diameter of 40 μm for the main channel and 20 μm for the drug inlet branch. The Reynolds number ratio of drug-inlet to main-channel flows is defined as

$$\chi = Re_2/Re_1 \tag{1}$$

The associated Reynolds numbers are

$$Re_i = \frac{(uD_h)_i}{v_i} \tag{2}$$

with $i = 1$ indicating the purging or nutrient-supply channel and $i = 2$ denoting the nanofluid channel (see Fig. 1b).

The drug concentration distribution for different main-channel lengths and inlet Reynolds numbers was analyzed. The effects of the Reynolds number ratio, χ, and thermal boundary condition, q_{wall}, were also compared and analyzed. Both the purging/nutrient-supply fluid and nano-drug solution were at inlet room temperature ($T_{in} = 293$ K).

2.1. Nanofluid property correlations

To evaluate the impact of nanoparticles (i.e., drugs) and wall heat flux on the velocity field as well as temperature and concentration profiles, the nanofluid properties have to be identified. Typically, for a very dilute suspension, the effective viscosity, density and specific heat capacity have the following forms (Xuan and Roetzel, [15]):

$$\mu_{eff} = \mu_f \frac{1}{(1-\varphi)^{2.5}} \tag{3}$$

$$\rho_{eff} = \varphi\rho_p + (1-\varphi)\rho_f \tag{4}$$

$$(\rho c_p)_{eff} = \varphi(\rho c_p)_p + (1-\varphi)(\rho c_p)_f \tag{5}$$

Here, ρ_{eff} is the nanofluid density, μ_{eff} is the nanofluid viscosity, and $(\rho c_p)_{eff}$ is the nanofluid specific heat capacity. The nanoparticle diffusivity follows the Stokes–Einstein equation:

$$D = \frac{\kappa_B T}{3\pi\mu d_p} \tag{6}$$

where κ_B is the Boltzmann constant, T is the fluid temperature, and d_p is the nanoparticle diameter.

Most challenging is the thermal conductivity of nanofluids, for which benchmark experimental data sets show that the thermal conductivity of a nanofluid has strong volume fraction as well as temperature dependences (Das et al., [16]; Li and Peterson, [17]). Some researchers introduced different effective thermal conductivity theories which directly or indirectly considered temperature dependence, e.g., Koo and Kleinstreuer [18], Prasher et al. [19], and Jang and Choi [20]. In comparison studies, Kleinstreuer and Li [21] and Li and Kleinstreuer [22] analyzed the models of Jang and Choi [20] and Prasher et al. [19], and updated their KKL (Koo–Kleinstreuer–Li) model. The KKL model is based on Brownian-motion-induced micro-mixing and achieved good agreements with various experimental data sets. Specifically, the KKL thermal conductivity model, k_{eff}, takes into account the effects of particle size, particle volume fraction and temperature dependence as well as the type of nanoparticle and base fluid combinations in form of (Koo and Kleinstreuer, [9]):

$$k_{eff} = k_{static} + k_{Brownian} \tag{7}$$

The static part is from Maxwell's model and the dynamic part was developed based on kinetic theory together with Stokes' flow of micro-scale convective heat transfer, i.e., micro-mixing. Hence,

$$\frac{k_{static}}{k_f} = 1 + \frac{3\left(\frac{k_{p,eff}}{k_f} - 1\right)\varphi}{\left(\frac{k_{p,eff}}{k_f} + 2\right) - \left(\frac{k_{p,eff}}{k_f} - 1\right)\varphi} \tag{8}$$

and

$$k_{Brownian} = 5 \times 10^4 \varphi\rho_f c_{p,f}\sqrt{\frac{\kappa_b T}{\rho_p d_p}}\, g\left(T, \varphi, d_p, \rho_p\right) \tag{9}$$

where ρ is the density, $c_{p,f}$ is fluid thermal capacity, and φ is the volume fraction, while the subscripts f and p indicate fluid and particle, respectively. The g-function, determined semi-empirically, was introduced to encapsulate the thermo-hydrodynamic interactions among all nanoparticles and affected micro-scale fluid parcels. For Al_2O_3–water and CuO–water nanofluids, the nonlinear g-function generated r^2 values of 96% and 98%, respectively (Li, [23]). The KKL model was employed in the current study.

2.2. Governing equations

Assuming the continuum approach to be valid (i.e., here $D_h \geqslant 20$ μm) for transient 3-D laminar incompressible flow in a microchannel, the continuity, momentum, energy and species transfer equations have to be solved, considering temperature-dependent fluid properties (see Section 2.1).

Continuity equation

$$\nabla \cdot [\rho(T)\vec{u}] = 0 \tag{10}$$

Momentum equation

$$\frac{\partial \vec{u}}{\partial t} + (\vec{u}\cdot\nabla\vec{u}) = -\frac{1}{\rho}\nabla p + \nabla\cdot(v\nabla\vec{u}) \tag{11}$$

Energy equation

$$\rho c_p\left[\frac{\partial T}{\partial t} + (\vec{u}\cdot\nabla)T\right] = \nabla^2(kT) + \mu\Phi \tag{12}$$

where

$$\Phi = \left(\frac{\partial u_i}{\partial x_j} + \frac{\partial u_j}{\partial x_i}\right)\frac{\partial u_i}{\partial x_j} \tag{13}$$

Mass transfer equation

$$\frac{\partial c}{\partial t} + \vec{u}\cdot\nabla c = D\nabla^2 c \tag{14}$$

Here, $\vec{u}$ is the velocity vector, D is the nanoparticle diffusivity, and Φ is the viscous dissipation function. For nanofluid flow and pure fluid flow, the corresponding physical properties will be chosen, i.e., the thermal conductivities, k_{eff} and k_f, respectively.

For the design analysis, uniform inlet velocity conditions and an ambient pressure condition for the outlet were applied. A 5% volume fraction of $d_p = 10$ and 500 nm nanoparticles in water was selected to enter the drug supply channel in the form of a rectangular pulse function. The cycle, shows as part of Fig. 1b, is centered with basically a one-second pulse during the observation time $t_T = 30$ s. It starts at dimensionless time $t^* = 0.49$, which is defined as

$$t^* = t/t_T, \quad 0 \leqslant t^* \leqslant 1 \tag{15}$$

where $t_T = L_{max}/u_1$ is the pulse period, and t is the real time, while $L_{max} = 10$ mm being the maximum length used, and $u_1 = \frac{v_1 Re_1}{D_{h_1}}$. A heat flux variable in magnitude and extent was applied along part of the bottom wall, starting at $z = 0.02$ mm and ending selectively at $z = 2.5$, 3, 4 or 5 mm (see Fig. 1b).

2.3. Numerical method

The numerical solution of the Eulerian transport equations were carried out with a user-enhanced, unstructured finite-volume based program, i.e., CFX 11 from Ansys, Inc. (Canonsburg, PA). The mesh size of the computational domain used in this study was refined until acceptable levels of grid independence of the solutions were achieved. Furthermore, both the maximum mass and momentum residuals were less than 10^{-4}.

3. Results

3.1. Model validations

Classical friction factor correlations as well as k_{eff}-comparisons are discussed. Specifically, for laminar fully-developed flow of a pure fluid, the Poiseuille number is defined as

$$Po = fRe = \frac{\Delta p \cdot D_h^2}{2\mu_f uL} \tag{16}$$

where Po = 16 for circular conduits.

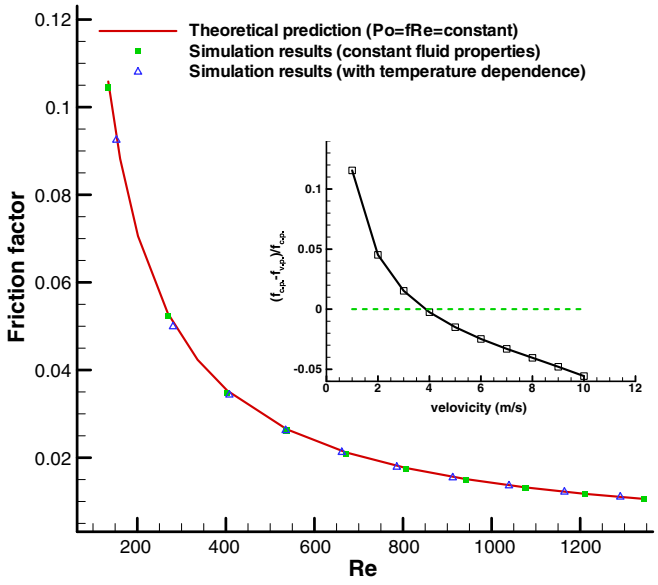

Fig. 2. Apparent friction factor vs. Reynolds number.

3.1.1. Friction factor

For rectangular microchannels, the Poiseuille number is a function of aspect ratio (α = channel width/channel height). It can be determined using Eq. (17) from Shah and London [24].

$$Po = 24(1 - 1.3553\alpha + 1.9467\alpha^2 - 1.7012\alpha^3 + 0.9564\alpha^4 - 0.2537\alpha^5) \tag{17}$$

where for square ducts, Po = 14.23. Fig. 2 provides a comparison of friction factors at different Reynolds number. Clearly, the computed friction factor is in very good agreement with the theoretical results. With an increase in inlet velocity, the temperature range and average temperature in the fluid decreases, i.e., from 304 K to 296 K, and the fluid kinematic viscosity increases. Thus, for the same velocity, the Reynolds number, $Re_1 = (\frac{uD_h}{\nu})_1$ is different for water with temperature-dependent properties when compared to constant properties. The reason is that the bottom heat flux influences the temperature distribution and, via the changing fluid properties, also the velocity field, especially where the temperature difference is large. The inset plot in Fig. 2 indicates the friction factor differences between water with temperature-dependent properties and constant properties for the same velocity. Specifically,

$$\varepsilon = \frac{(f_{c.p} - f_{v.p})}{f_{c.p}} \tag{18}$$

where $f_{c.p}$ is the friction factor for water with constant properties, $f_{v.p}$ is the friction factor for water with variable properties, i.e., temperature dependent. In the lower velocity range, the higher fluid temperature induced a lower kinematic viscosity for the temperature-dependent fluid which introduced a higher Reynolds number and hence a smaller friction factor. As the velocity increases, the friction factor increases because of the decrease in the fluid's average temperature. Fig. 3a and b show the axial velocity distribution at the channel outlet for water with temperature-dependent and constant properties, respectively. As Fig. 3a indicates, the temperature generated a decrease in viscosity near the bottom surface and as a result lowers the location of the maximum velocity, while for water with constant properties the maximum velocity always appears at the centerline (see Fig. 3b).

3.1.2. Pressure gradient

Li and Kleinstreuer [22] analyzed the influence of nanoparticle volume fraction on the pressure gradient for fully-developed flow. Selecting nanofluids with 4% volume fractions of 28.6 nm CuO–water mixtures, the pressure gradient increased an average 13% for a constant flow rate, which matched measured data. Fig. 4 depicts the pressure gradients at different mean velocities when employing a 5% gold-particle-and-water mixture with different

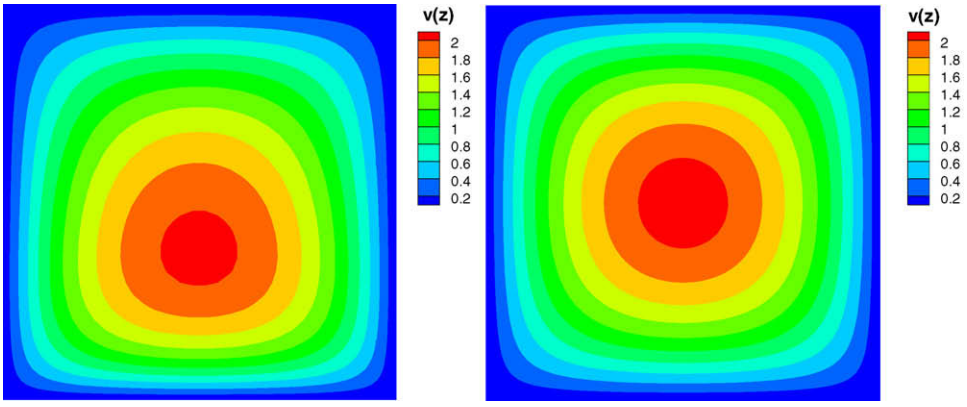

Fig. 3. Velocity distribution in channel outlet (a) water with temperature dependent properties and (b) water with constant physical properties.

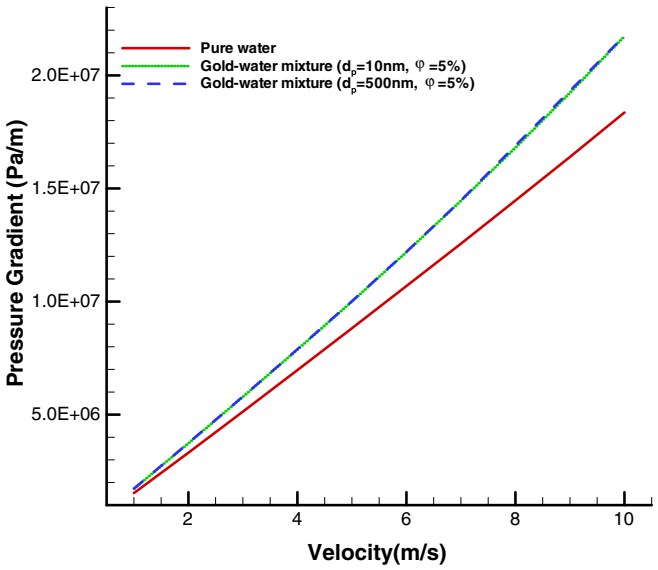

Fig. 4. Pressure gradient vs. velocity.

nanoparticle sizes, i.e., 10 and 500 nm (see Labhasetwar & Leslie-Pelecky, [14]). Clearly, nanoparticle size does not influence the pressure gradient when the same volume fraction is employed (see Eqs. (3)–(5)). The pressure gradient increases by 13–18% when employing the 5% nanofluids, confirming the results of Li and Kleinstreuer [22].

3.1.3. Enhanced thermal conductivity

In Fig. 5, the KKL model is compared with experimental data for CuO–water nanofluid at different temperatures (21 °C, 36 °C, 51 °C) and volume fractions (1–4%). The KKL model compares well with the experimental observations of Das et al. [16]. Because of the lack of quantitative information concerning therapeutic nanoparticles, other than their mean diameters, the practical range for k_{eff}/k_f was assumed to be 1.0–2.5 and the g-function was taken to be linearly dependent on temperature (20–70 °C), generating a value range for g of 0.3×10^{-3} to 7×10^{-3}.

3.2. Concentration distributions of drug nano-particles

The distributions of nanoparticle concentrations and temperatures at the main microchannel outlets with variable channel lengths were compared for different particle sizes and boundary conditions, i.e., different Reynolds numbers Re_1 and Re_2 and for different Reynolds numbers ratios χ as well as different heating modes q_w. The desired nano-drug particle uniformity at $z = L$ is defined as

$$U_c = A_v/A_g \times 100\% \tag{19}$$

where A_v is the valid area, i.e., the area where the drug particle concentration is equal or larger than 90% of local maximum concentration, and A_g is the actual geometric channel-exit area. Fig. 6 compares the dimensionless drug concentration distributions ($d_p = 10$ nm) at different cross sections in the microchannel for different times. Comparing the $U_c(t)$ graphs for the outlet cross section at $z = 10$ mm, it is evident that the added heat measurably increases nanoparticle diffusion $\left(D = \frac{\kappa_B T}{3\pi\mu d_p}\right)$ and hence the drug distribution two-fold, i.e., via the mixture temperature and the reduced fluid viscosity. At station $z = 3$ mm, the nanoparticles are still concentrated in a small part of the channel cross section and hence the drug uniformity U_c is very low. Clearly, nanoparticle (i.e., drug) mixing develops as the two streams merge, and for $z = 10$ mm the desired near-uniform concentration profile is achieved. There, the difference is less than 10% between the maximum value and the minimum value in the particular cross section.

Figs. 7a–d and 8a–d depict the velocity and dimensionless nano-drug concentration distributions along the center line ($-2 \times 10^{-5} \leqslant y \leqslant 2 \times 10^{-5}$) at three flow-developing phases ($z = 0.5$ mm, 5 mm and 10 mm) at different time levels for the case of $\chi = 1.69$ and $L = 10$ mm. The dimensionless nano-drug concentration is defined as:

$$c^* = c/c_0 \tag{20}$$

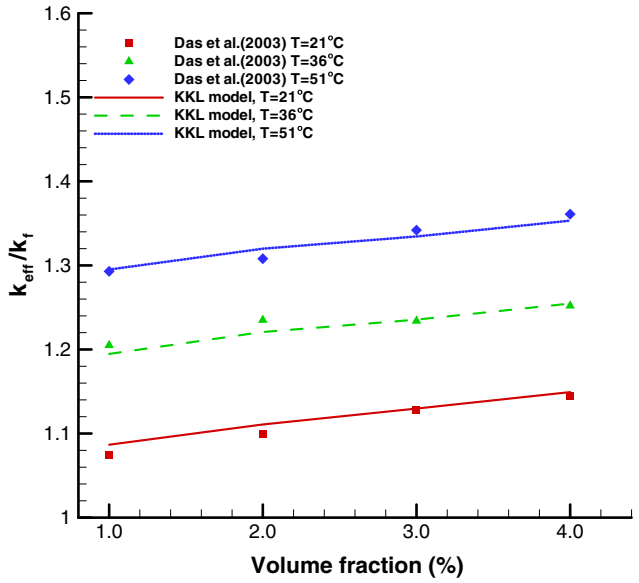

Fig. 5. Comparison of KKL model with experimental data of Das et al. [16] for CuO–water mixture.

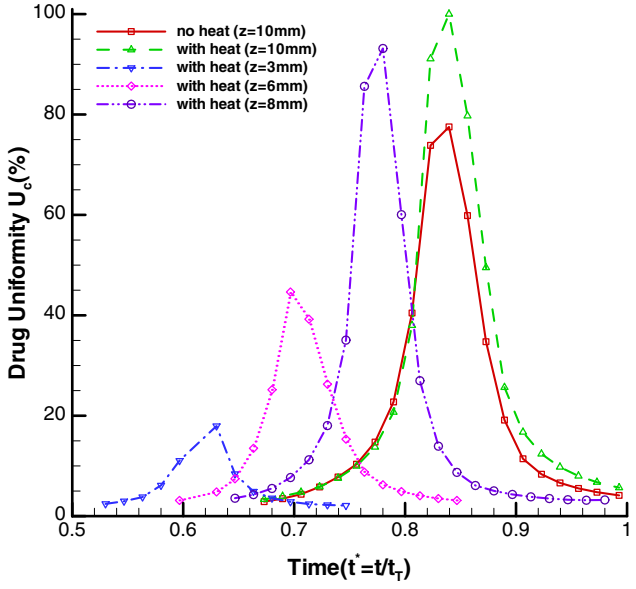

Fig. 6. Comparison of drug concentration uniformity for different thermal boundary conditions in outlet planes and/or different axial stations ($d_p = 10$ nm).

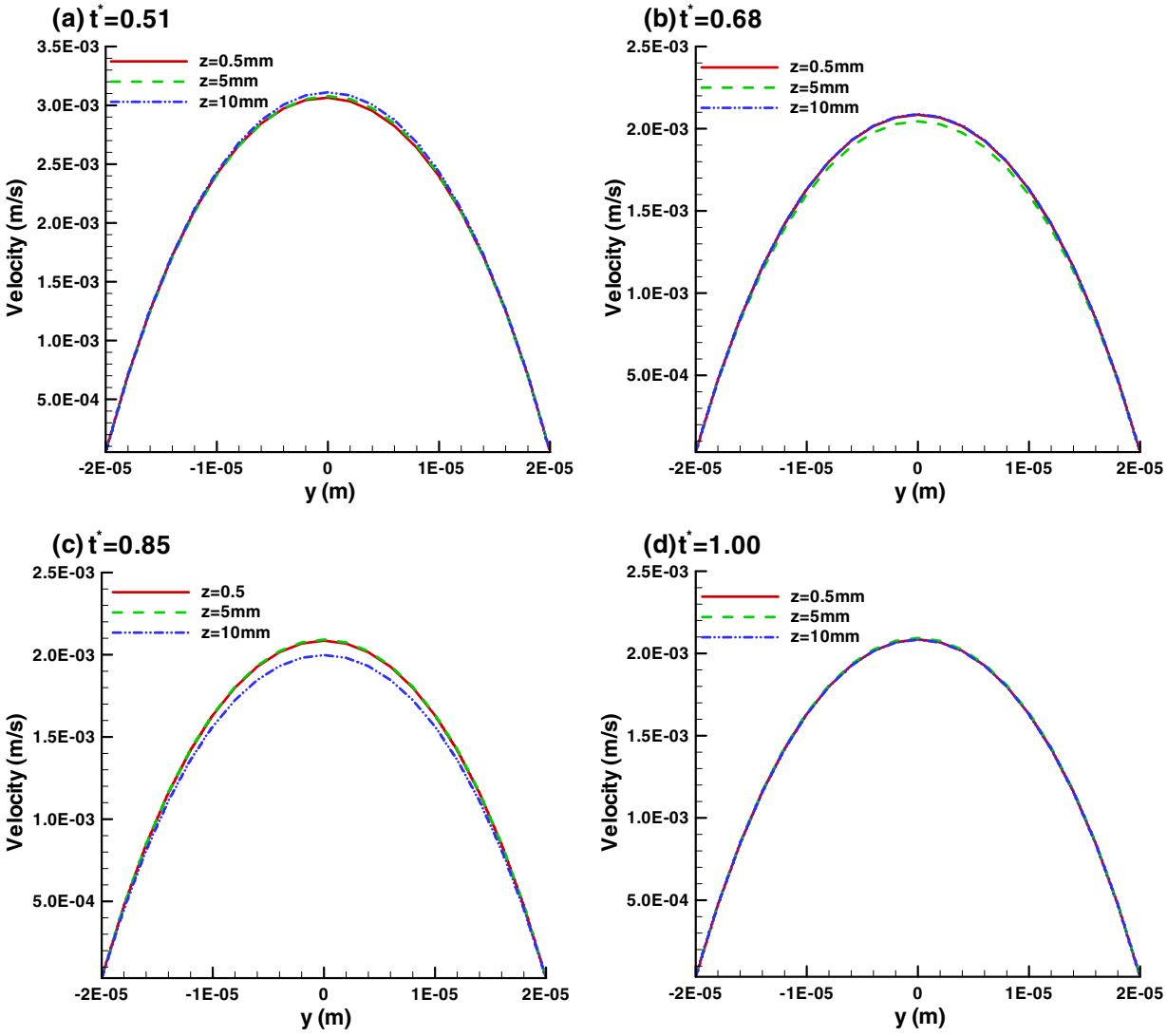

Fig. 7. Comparison of velocity profiles in the main microchannel at different phases of mixture flow evolution at stations $z = 0.5$, 5 and 10 mm ($d_p = 10$ nm, and $\chi = 1.69$).

here c is the local drug concentration, and c_0 is the drug concentration at the drug-channel inlet, which is assumed to be unity.

The intensity of drug supply measurably influences the velocity distribution (Fig. 7). At $t^* = 0.51$, in the middle of nanofluid injection, the main-channel velocity is at a maximum. The velocity down stream of $z > 0.5$ mm is somewhat elevated because of the nano-drug influence (see Fig. 8a). For the same reason, at $t^* = 0.68$ and $t^* = 0.85$, the velocity distribution exhibits the lowest values at $z = 5$ mm and $z = 10$ mm, respectively (Fig. 7b and c). At $t^* = 1.0$, most of the nano-drug particles supplied have left the delivery microchannel and hence the velocity distributions at the three axial stations (i.e., $z = 0.5$, 5, and 10 mm) exhibit no differences any more (Fig. 7d).

At the middle of the one-second nanofluid cycle (i.e., $t^* = 0.51$), the resulting nano-drug pulse is registered near the inlet at $z = 0.5$ mm but is not felt further downstream (Fig. 8). The nanoparticles diffuse and they are conveyed through the channel leading to highly nonlinear "time- and space-"dependent concentration profiles (Fig. 8a–d). For example, at $t^* = 0.85$ the nano-drug distribution is almost uniform across the channel exit plane (see Fig. 8c).

Fig. 9 compares the uniformity of drug-particle concentration at different Re_1 numbers and microchannel lengths. With the decrease of Re_1 values from 0.04 to 0.004 and with an increase of the channel length, which implies much larger diffusion times, the uniformity of drug-particle distribution improves. As expected, at small Reynolds numbers, drug uniformity can be much more rapidly achieved.

Fig. 10 depicts the drug uniformity at channel outlet $z = 10$ mm for drugs with a particle diameter of 500 nm at different Reynolds numbers. It shows that the decrease of Re_1 can improve drug uniformity. Comparison of Figs. 10 and 6 shows that smaller drug-particles may greatly benefit the drug concentration uniformity.

Figs. 11 and 12 summarize the percentage changes in minimum microchannel-length in order to achieve near-uniform exit concentration for different Reynolds number ratios and different wall-heat-flux extents, respectively. The "minimum uniformity-length" is defined as the required main-channel length where the drug-particle concentration in the exit area is equal or larger than 90% of the local maximum concentration. Selecting $\chi = 1.26$ as the reference ratio, the dimensionless minimum uniformity length change is compared for different Reynolds number ratios in Fig. 11, an increase of χ measurably decreases the minimum uniformity length. As Fig. 12 shows, a decrease of the heated area also decreases the minimum uniformity length. Because the fluid temperature increase is fixed (from room temperature 293 K to body

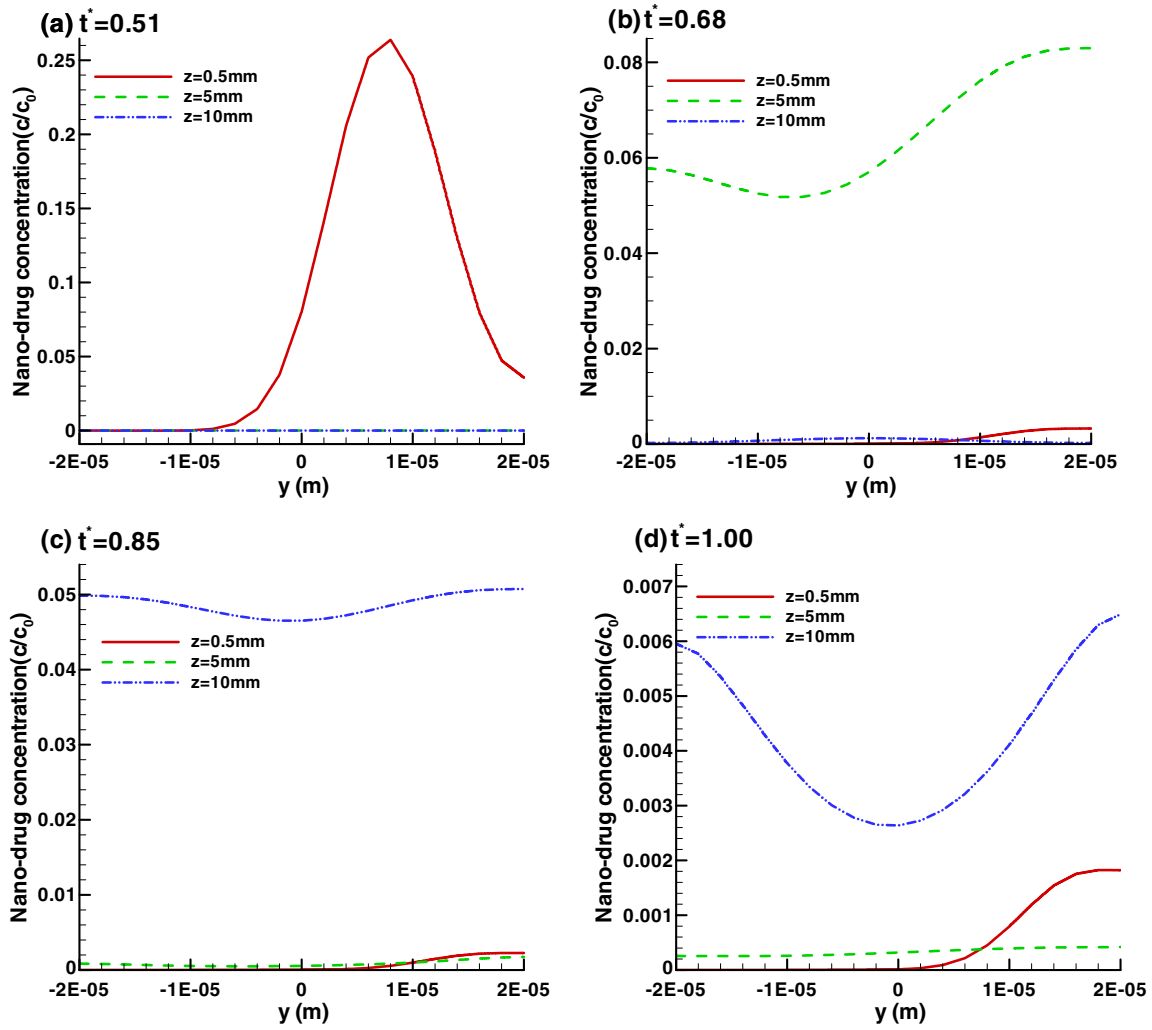

Fig. 8. Comparison of nano-drug concentration distributions in the main microchannel at different phases of mixture flow evolution at stations $z = 0.5$, 5 and 10 mm ($d_p = 10$ nm, and $\chi = 1.69$).

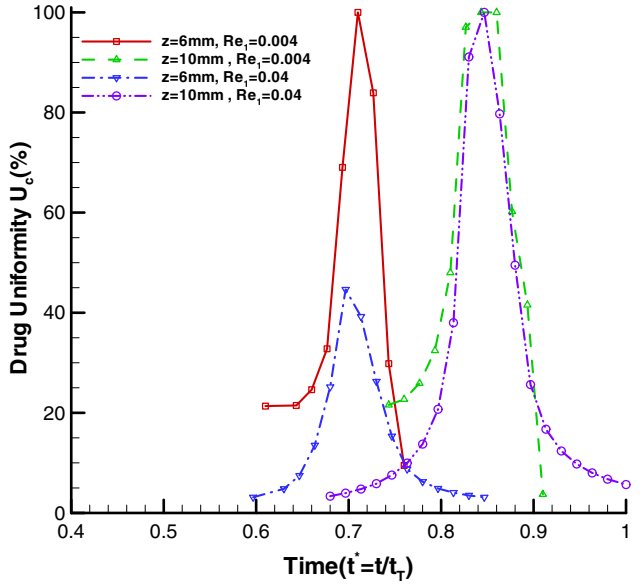

Fig. 9. Comparison of drug-concentration uniformity at different microchannel lengths for different Reynolds numbers ($d_p = 10$ nm).

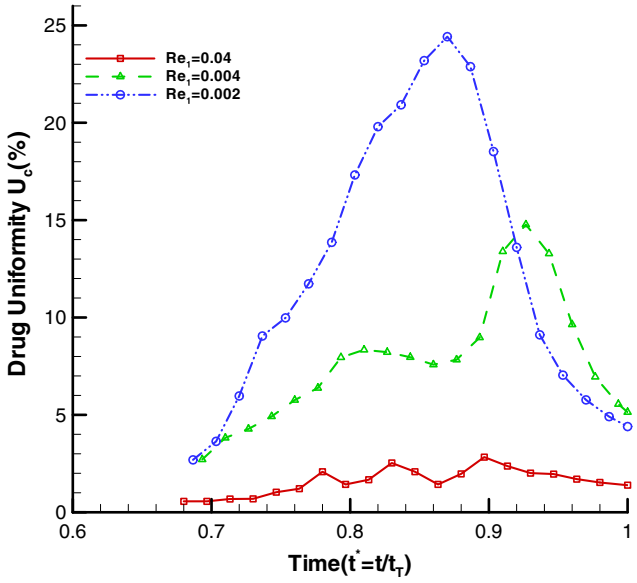

Fig. 10. Comparison of drug-concentration uniformity in the outlet plane at $z = 10$ mm for different Reynolds numbers ($d_p = 500$ nm).

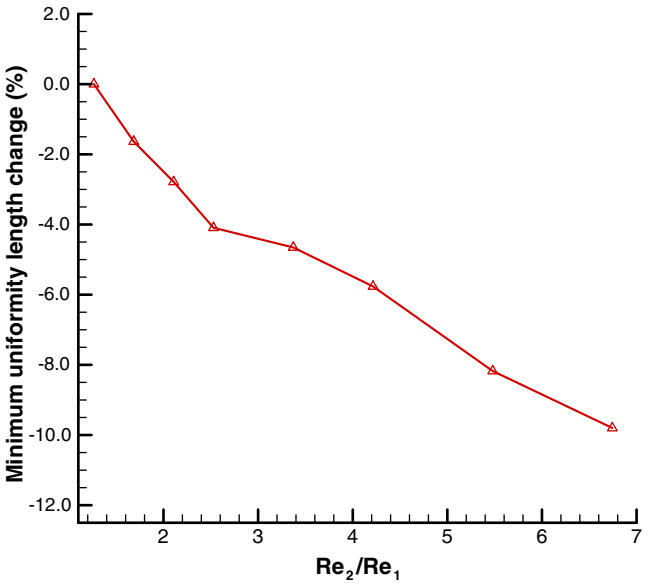

Fig. 11. Minimum uniformity length as a function of Reynolds number ratio (d_p = 10 nm).

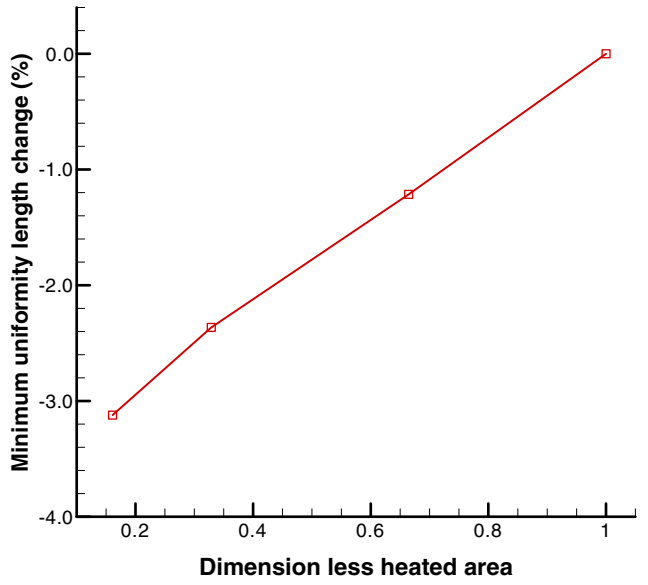

Fig. 12. Minimum uniformity length as a function of dimensionless heated area (d_p = 10 nm).

temperature 310 K), the effect on the drug diffusivity is not prominent by just decreasing the heated area.

4. Conclusions

In the present study a nano-drug-supply system, i.e., a bio-MEMS, was introduced. Of main interest were the conditions for achieving uniform concentrations at the microchannel exit of the supplied nano-drugs. A heat flux which depends on the levels of nano-fluid and purging fluid velocity was added to ensure that drug delivery to the living cells occurs at an optimal temperature, i.e., 37 °C. The added wall heat flux had also a positive influence on drug-concentration uniformity. Overall, the nano-drug concentration uniformity is influenced by channel length, particle diameter and the Reynolds number of both the nanofluid supply and main microchannels. In light of the convection–diffusion controlled transport mechanisms, longer channels, smaller particle diameters as well as lower Reynolds numbers are desirable for best, i.e., uniform drug delivery. Furthermore, the Reynolds number ratio and the extent of heated area also measurably influence the minimum microchannel length required for achieving the desired drug-concentration uniformity. Future work will focus on the effects of angled drug-delivery channel and static mixer in the main channel.

Acknowledgement

The support of Jie Li via an endowed fellowship created by Joe and Sarah Archie as well as the use of ANSYS-CFX11 (Ansys, Inc., Canonsburg, PA) are gratefully acknowledged.

References

[1] H.A. Stone, A.D. Stroock, A. Ajdari, Engineering flows in small devices: microfluidics toward a lab-on-a-chip, Annu. Rev. Fluid Mech. 36 (2004) 381–411.
[2] C. Kleinstreuer, J. Li, in: D. Li (Ed.), Microscale Cooling Devices, Encyclopedia of Micro and Nanofluidic, Springer-Verlag, Heidelberg, DE, 2008.
[3] P. Tabeling, Introduction to Microfluidics, Oxford University Press, Oxford, UK, New York, 2005.
[4] N.-T. Nguyen, S.T. Wereley, Fundamentals and Applications of Microfluidics, Arten House, Boston, 2006.
[5] F.E.H. Tay, Microfluidics and Biomems Applications, Kluwer Academic Publishers, Boston, 2002.
[6] Steven S. Saliterman, Fundamentals of BioMEMS and Medical Microdevices, Wiley-Interscience SPIE PRESS Bellingham, Washington, USA, 2006.
[7] W. Wang, S.A. Soper, Bio-MEMS: Technologies and Applications, CRC/Taylor & Francis, Boca Raton, 2006.
[8] D.J. Beebe, G.A. Mensing, G.M. Walker, Physics and applications of microfluidics in biology, Annu. Rev. Biomed. Eng. 4 (2002) 261–286.
[9] J. Koo, C. Kleinstreuer, Liquid flow in microchannels: experimental observations and computational analysis of microfluidics effect, J. Micromech. Microeng. 13 (2003) 568–579.
[10] R.S. Shawgo, A.C.R. Grayson, Y. Li, M.J. Cima, Bio-MEMS for drug delivery, Curr. Opin. Solid State Mater. Sci. 6 (2002) 329–334.
[11] Cepheid, <http://www.Cepheid.Com>, 2003.
[12] A. Ovsianikov, B. Chichkov, et al., Two photon polymerization of polymer–ceramic hybrid materials for transdermal drug delivery, Int. J. Ceramic Technol. 4 (2007) 22–29.
[13] K. Kim, J.B. Lee, High aspect ratio tapered hollow metallic microneedle arrays with microfluidic interconnector, Microsyst. Technol. 13 (2007) 231–235.
[14] V. Labhasetwar, D.L. Leslie-Pelecky, Biomedical Applications of Nanotechnology, Wiley-Interscience, A John Wiley & Son, Inc., Publication, 2007.
[15] Y. Xuan, W. Roetzel, Conceptions for heat transfer correlation of nanofluids, Int. J. Heat Mass Transfer 43 (2000) 3701–3707.
[16] S.K. Das, N. Putra, P. Thiesen, W. Roetzel, Temperature dependence of thermal conductivity enhancement for nanofluids, J. Heat Transfer 125 (2003) 567–574.
[17] C.H. Li, G.P. Peterson, Experimental investigation of temperature and volume fraction variations on the effective thermal conductivity of nanoparticle suspensions (nanofluids), J. Appl. Phys. 99 (2006) 084314.
[18] J. Koo, C. Kleinstreuer, A new thermal conductivity model for nanofluids, J. Nanoparticle Res. 6 (2004) 577–588.
[19] R.S. Prasher, P. Bhattacharya, P.E. Phelan, Brownian motion based convective conductive model for the effective thermal conductivity of nanofluids, J. Heat Transfer 128 (2006) 588–595.
[20] S.P. Jang, S.U.S. Choi, Effects of various parameters on nanofluid thermal conductivity, J. Heat transfer 129 (2007) 617–623.
[21] C. Kleinstreuer, J. Li, Analysis of the Jang & Choi k_{eff}-model, ASME J. Heat Transfer 130 (2008).
[22] J. Li, C. Kleinstreuer, Thermal performance of nanofluid flow in microchannels, Int. J. Heat Fluid Flow, 29 (2008), in press.
[23] J. Li, Computational Analysis of Nanofluid Flow in Microchannels with Applications to Micro-heat Sinks and Bio-MEMS, Ph.D. dissertation, MAE Department, NCSU, Raleigh, NC, 2009.
[24] S.K. Shah, A.L. London, Laminar Flow Forced Convection in Ducts, Supplement 1 to Advances in Heat Transfer Academic, New York, 1978.